


ORIGINAL RESEARCH

Open Access



First-in-human use of ^{11}C -CPPC with positron emission tomography for imaging the macrophage colony-stimulating factor 1 receptor

Jennifer M. Coughlin^{1,2†}, Yong Du^{2†}, Wojciech G. Lesniak², Courtney K. Harrington¹, Mary Katherine Brosnan², Riley O'Toole¹, Adeline Zandi², Shannon Eileen Sweeney¹, Rehab Abdallah², Yunkou Wu², Daniel P. Holt², Andrew W. Hall², Robert F. Dannals², Lilja Solnes², Andrew G. Horti² and Martin G. Pomper^{1,2*} 

Abstract

Purpose: Study of the contribution of microglia to onset and course of several neuropsychiatric conditions is challenged by the fact that these resident immune cells often take on different phenotypes and functions outside the living brain. Imaging microglia with radiotracers developed for use with positron emission tomography (PET) allows researchers to study these cells in their native tissue microenvironment. However, many relevant microglial imaging targets such as the 18 kDa translocator protein are also expressed on non-microglial cells, which can complicate the interpretation of PET findings. ^{11}C -CPPC was developed to image the macrophage colony-stimulating factor 1 receptor, a target that is expressed largely by microglia relative to other cell types in the brain. Our prior work with ^{11}C -CPPC demonstrated its high, specific uptake in brains of rodents and nonhuman primates with neuroinflammation, which supports the current first-in-human evaluation of its pharmacokinetic behavior in the brains of healthy individuals.

Methods: Eight healthy nonsmoker adults completed a 90-min dynamic PET scan that began with bolus injection of ^{11}C -CPPC. Arterial blood sampling was collected in order to generate a metabolite-corrected arterial input function. Tissue time-activity curves (TACs) were generated using regions of interest identified from co-registered magnetic resonance imaging data. One- and two-tissue compartmental models (1TCM and 2TCM) as well as Logan graphical analysis were compared.

Results: Cortical and subcortical tissue TACs peaked by 37.5 min post-injection of ^{11}C -CPPC and then declined. The 1TCM was preferred. Total distribution volume (V_T) values computed from 1TCM aligned well with those from Logan graphical analysis ($t^* = 30$), with V_T values relatively high in thalamus, striatum, and most cortical regions, and with relatively lower V_T in hippocampus, total white matter, and cerebellar cortex.

Conclusion: Our results extend support for the use of ^{11}C -CPPC with PET to study microglia in the human brain.

Keywords: Human PET neuroimaging, Microglia, CSF1R, Neuroinflammation, PET

Introduction

Imaging of microglia and their contribution to brain injury and repair across neuropsychiatric conditions has been widely pursued [1, 2]. Radiotracers developed for use with positron emission tomography (PET) can allow researchers to study microglia in their native tissue

[†]Jennifer M. Coughlin and Yong Du contributed equally to this work.

*Correspondence: mpomper@jhmi.edu

¹ Department of Psychiatry and Behavioral Sciences, Johns Hopkins Medical Institutions, Baltimore, MD, USA

Full list of author information is available at the end of the article

microenvironment [3–5], which has advantages since these resident immune cells assume different morphologies *ex vivo* [6]. However, relevant microglial targets such as 18 kDa translocator protein may be expressed on other cell types in human brain [4, 5, 7]. We developed ^{11}C -CPPC to image the macrophage colony-stimulating factor 1 receptor (CSF1R), which is expressed almost exclusively by microglia in the brain [8].

CSF1R is a type III tyrosine kinase receptor that is activated by binding of its endogenous ligands, colony-stimulating factor 1 or interleukin 34 [9]. There is no clear human brain region devoid of the receptor, and CSF1R RNA expression has been reported in many brain regions including thalamus, cerebral cortex, cerebellum, white matter, and hippocampus [10]. CSF1R signaling plays a role in the survival, homeostatic functions, and proliferation of microglia, and its expression may be higher in the brains of patients with certain neurologic conditions such as Alzheimer's disease or amyotrophic lateral sclerosis [11]. Existing and emerging inhibitors of CSF1R may prevent neurodegeneration in models of Alzheimer's disease [12] and traumatic brain injury [13, 14], which supports further research into the therapeutic potential of CSF1R antagonism in select neurologic conditions.

^{11}C -CPPC [8] is an isotopolog of the selective CSF1R inhibitor, 5-cyano-N-(4-(4-methylpiperazin-1-yl)-2-(piperidin-1-yl)phenyl)furan-2-carboxamide [15]. Unlabeled CPPC has beneficial properties to promote blood–brain barrier permeability such as ideal lipophilicity [calculated partition coefficient (clogD7.4) of 1.6] and molecular mass of 393 Da [8]. We recently demonstrated high, specific uptake of ^{11}C -CPPC in murine and nonhuman primate models of neuroinflammation [8] and now present its first-in-human use with PET. This study assessed the pharmacokinetic behavior of ^{11}C -CPPC in the brains of eight healthy individuals. Estimates of regional kinetic parameters and total distribution volume (V_T) values were generated using pharmacokinetic modeling methods with a metabolite-corrected arterial input function, and the different model fits were compared.

Materials and methods

Human subjects

The Johns Hopkins Institutional Review Board approved this study, and all research participants provided written, informed consent. Adult (≥ 18 years of age) individuals completed a screening clinical research interview and laboratory testing (blood counts, metabolic panel, coagulation studies, pregnancy testing when applicable) with electrocardiogram and urine toxicology. Eligible participants were assessed as being in stable health with no clinical abnormality on the screening assessment and structural magnetic resonance imaging (MRI). A Johns

Hopkins faculty neuroradiologist reviewed each structural MRI. Exclusion criteria included use of cannabis, nicotine, or other recreational substances in the past six months (assessed by self-report and urine toxicology), prescribed or over-the-counter anti-inflammatory medication within two weeks prior to the PET, acute onset or exacerbation of illness/infection in the past month, contraindication to MRI, or contraindication to PET imaging with an arterial line.

Human brain imaging

Synthesis of ^{11}C -CPPC

^{11}C -CPPC was synthesized as described by Mathews et al. [16] at the Johns Hopkins PET Radiotracer Center. The synthesis and all major quality measures (including radiochemical purity $>95\%$) were in compliance with standard good manufacturing practice for PET radiotracers. Molar activity of ^{11}C -CPPC at the time of injection was 316.8 ± 138.8 GBq/ μmol . The mean administered mass and radioactivity of ^{11}C -CPPC were 1.2 ± 1.1 μg (range 0.55–3.72 μg) and 651.4 ± 62.8 MBq (range 542.8–736.7 MBq), respectively.

MRI acquisition and regions of interest

A T1-weighted Magnetization-Prepared Rapid Gradient-Echo (MP-RAGE) sequence with $0.75 \times 0.75 \times 0.8$ mm voxel size was acquired from each participant using a 3 Tesla MRI system (Siemens MAGNETOM Prisma, Malvern, PA, USA or Philips Achieva, Best, Netherlands). MRI data were segmented using the FreeSurfer image analysis suite (<http://surfer.nmr.mgh.harvard.edu/>). Ten regions of interest (ROIs) were selected: total white matter, thalamus, striatum, hippocampus, as well as cerebellar, temporal, occipital, cingulate, frontal, and parietal cortices (Additional file 1: Fig. S1).

PET acquisition and reconstruction

Before the PET, each participant underwent fitting of a thermoplastic facemask, as well as insertion of a radial arterial catheter and intravenous catheter. The thermoplastic facemask was used for head fixation during the PET to minimize head motion. An attenuation map was estimated from a 6 min transmission scan that was performed with a ^{137}Cs point source prior to the emission scan. Each emission scan started at the time of bolus intravenous injection of ^{11}C -CPPC, with continuous list mode data collection for 90 min on a High Resolution Research Tomograph (Siemens Healthcare, Knoxville, TN) [17]. Imaging data were reconstructed using the iterative ordinary-Poisson ordered-subset expectation–maximization algorithm (6 iteration and 16 subsets, 2 mm post-smoothing) and were corrected for decay, attenuation, random activity, and scatter [18].

The reconstructed data were binned into 30 frames (four 15 s, four 30 s, three 1 min, two 2 min, five 4 min, and twelve 5 min). The reconstructed image volume spanned 31 cm × 31 cm transaxially and 25 cm axially, with image matrix of 256 × 256 × 207 voxels (voxel size of 1.22 × 1.22 × 1.22 mm).

Plasma acquisition

Arterial whole blood samples were collected manually over the course of the emission scan. First, 7 ml of blood were drawn for the protein binding sample and 4 ml of blood were drawn for the pre-injection/background high-performance liquid chromatography (HPLC) measurement. Then, 1 ml blood samples were collected from (a) time of injection to 1.5 min post-injection (p.i.) at a rate as fast as possible (a total of 16–18 samples); (b) 1.5–3 min p.i. every 30 s; (c) 3–5 min p.i. every 2 min; (d) 5–30 min p.i. every 5 min; and (e) from 30 to 90 min p.i. every 15 min. An additional volume of 3–6 mL was drawn at the 5, 10, 20, 30, 60, and 90 min time points for HPLC measurements. Plasma was immediately isolated from each blood sample using centrifugation before plasma radioactivity was counted in a cross-calibrated gamma well-counter (PerkinElmer 2480 WIZARD2 Automatic Gamma Counter, Shelton, CT). The previously described modified column-switching HPLC method was used to measure the fraction of parent ^{11}C -CPPC in plasma at 5, 10, 20, 30, 40, 60, and 90 min p.i. [8]. Metabolite-corrected time-activity curves (TACs) were generated by applying the parent ^{11}C -CPPC fraction to the total plasma TACs using linear interpolation (v3.7, PMOD Technologies Ltd., Zurich, Switzerland). Ultrafiltration (Centrifree Ultrafiltration Device, MilliporeSigma, Burlington, MA) was used to measure plasma free fraction (f_p) of ^{11}C -CPPC.

PET data processing

PET data preprocessing steps as well as the kinetic analyses were conducted using PMOD (v3.7, PMOD Technologies Ltd., Zurich, Switzerland). Post-reconstruction inter-frame motion correction was applied as needed by frame-by-frame matching of dynamic data to a static reference frame generated from the average of the frames corresponding to 30–60 min p.i. PET data were rigidly transformed into MR space by co-registering the mean 30–60-min PET image and each of the 30 motion-corrected PET frames to the T1-weighted MRI image.

Derivation of PET rate constants and distribution volumes

Total distribution volume, V_T [19], for each ROI was derived using the metabolite-corrected arterial input function and compartmental modeling (one-tissue compartment model with 3 parameters, 1TCM; two-tissue

compartment model with 4 parameters, 2TCM) or Logan graphical analysis [20]. The delay between the input function and tissue signal was estimated using a fit for the whole brain and then fixed across the ROI fits. Across participants, the mean estimated delay was < 2 s. Cerebral blood volume was set to 5% of brain volume in compartmental models, with $C_{\text{model}}(t) = (1 - vB) * C_T(t) + vB * C_p(t)$, wherein C_{model} is the modeled curve, vB is blood volume fixed at 0.05, C_T is the measured tissue activity, and C_p is measured plasma activity. Nonlinear least squares regression was used to calculate the parameters of the compartmental models and the % standard error (%SE) of each estimated parameter. In Logan graphical analysis, various selections of equilibration time, t^* , were evaluated across the ROIs using the 10% max error criterion, with ultimate selection of $t^* = 30$ min.

Statistics

The compartmental model fits that were applied to the regional TACs were first assessed visually before the relative goodness of fit was assessed using the F test [21]. Regional V_T estimates from variable scan durations were evaluated against those V_T values estimated from the full 90-min acquisition through data shortening in 5 min intervals down to a 50-min continuous scan duration p.i. For each duration, denoted X , relative bias values were expressed as $|V_{TX} - V_{T90\text{min}}| / V_{T90\text{min}}$. Data are presented as mean ± standard deviation unless otherwise noted.

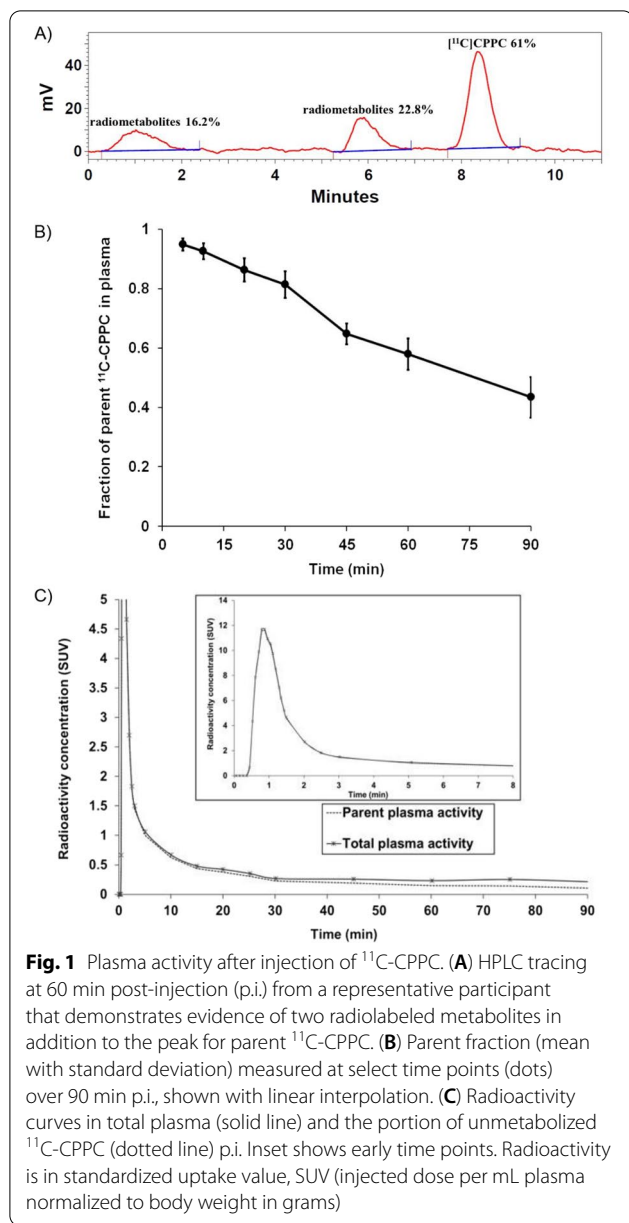
Results

Human subjects

Eight healthy nonsmokers (four males, four females, age range 24–65 years, median 42 years, interquartile range 22 years) underwent PET neuroimaging with ^{11}C -CPPC. Participants were of Caucasian ($N=4$), African-American ($N=2$), or Asian ($N=2$) race and had mean body weight of 81.8 ± 17.2 kg. Based on assessments that included monitoring of vital signs, laboratory testing, and electrocardiograms, there were no adverse or clinically detectable pharmacologic effects from injection of ^{11}C -CPPC. Scores on assessments probing signs and symptoms of depression, anxiety, and cognitive impairment were consistent with absence of active neuropsychiatric illness ($N=8$), with mean Hamilton Depression Rating Scale Score of 0.6 ± 0.9 , mean Hamilton Anxiety Rating Scale Score of 0.9 ± 1.1 , and mean Mini Mental Status Exam score of 29.8 ± 0.5 .

Plasma analysis

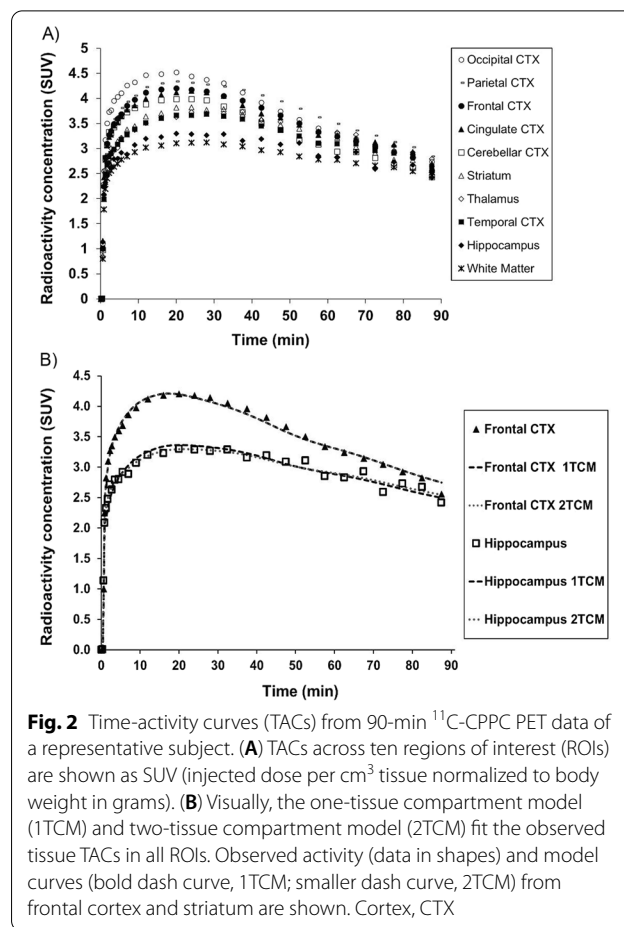
HPLC revealed two radiolabeled metabolites that were more polar than the parent, ^{11}C -CPPC (Fig. 1A). The parent fraction decreased moderately over the 90 min p.i.,



with parent ^{11}C -CPPC fraction representing $57.9 \pm 5.3\%$ and $43.4 \pm 6.8\%$ of total plasma activity by 60 min and 90 min, respectively (Fig. 1B). Total plasma activity peaked within 60 s p.i. (Fig. 1C). Measured f_p was $3.26 \pm 0.57\%$.

Derivation of kinetic rate constants and V_T

Over the 90-min scan duration, regional radioactivity curves peaked within 37.5 min p.i. of ^{11}C -CPPC and then declined (Fig. 2A). Highest peak uptake occurred in



cortical regions and thalamus, with slightly lower peaks in hippocampus and total white matter.

Visually, each compartmental model fit the regional TACs well (Fig. 2B). The 1TCM was able to estimate individual parameters (K_1 , k_2) and V_T well (Table 1). The 2TCM estimated V_T well except for one unstable white matter V_T estimate from one individual (Table 1). The 2TCM was statistically favored over the 1TCM in 45% of fits by the F test. However, the 2TCM did not identify several individual parameters well, as evidenced by K_1 with $\text{SE} > 10\%$ in 16.3% of fits, and k_2 , k_3 , and k_4 each with $\text{SE} > 5\%$ in the majority of fits. After excluding the one unstable white matter V_T value from 2TCM, regional V_T from the 1TCM aligned with V_T estimates from the 2TCM ($1\text{TCM } V_T = 1.02 * 2\text{TCM } V_T - 0.47$, $R^2 = 0.99$). The 1TCM was therefore selected as the preferred compartmental model for regional V_T estimates of ^{11}C -CPPC PET data. Since Logan-derived V_T estimates aligned well with regional V_T from the 1TCM (Logan $V_T = 0.88 * 1\text{TCM } V_T + 1.07$, $R^2 = 0.92$), Logan analysis was also appropriate for quantitative estimation of V_T . Representative regional Logan plots are shown in Fig. 3. V_T

Table 1 Kinetic parameters and total distribution volume (V_T) values estimated with the one-tissue compartment model (1TCM), along with V_T values estimated using two-tissue compartment model (2TCM), and Logan analysis for ^{11}C -CPPC PET imaging in humans ($N=8$)

Region of interest	1TCM			2TCM	Logan
	K_1 ($\text{mL cm}^{-3} \text{ min}^{-1}$)	k_2 (min^{-1})	V_T (mL cm^{-3})	V_T (mL cm^{-3})	V_T (mL cm^{-3})
Thalamus	0.29 ± 0.04 (0.97)	0.02 ± 0.00 (1.99)	16.6 ± 2.0 (1.34)	16.9 ± 2.1 (1.92)	16.0 ± 2.0 (1.26)
Striatum	0.30 ± 0.04 (0.96)	0.02 ± 0.00 (1.94)	16.2 ± 1.8 (1.30)	16.3 ± 1.9 (3.11)	15.2 ± 1.8 (1.28)
Parietal cortex	0.32 ± 0.03 (0.80)	0.02 ± 0.00 (1.54)	16.1 ± 1.7 (1.02)	16.2 ± 1.7 (1.85)	15.2 ± 1.5 (0.70)
Cingulate cortex	0.31 ± 0.04 (0.92)	0.02 ± 0.00 (1.78)	15.7 ± 2.0 (1.18)	15.8 ± 2.0 (2.68)	14.9 ± 1.9 (1.09)
Temporal cortex	0.26 ± 0.03 (0.92)	0.02 ± 0.00 (1.96)	15.6 ± 1.8 (1.33)	15.7 ± 1.8 (3.04)	14.7 ± 1.6 (1.10)
Frontal cortex	0.32 ± 0.04 (0.85)	0.02 ± 0.00 (1.60)	15.2 ± 1.5 (1.06)	15.3 ± 1.5 (1.31)	14.5 ± 1.5 (0.92)
Occipital cortex	0.31 ± 0.02 (0.90)	0.02 ± 0.00 (1.71)	14.9 ± 1.7 (1.13)	15.0 ± 1.7 (1.92)	14.1 ± 1.5 (0.65)
Hippocampus	0.22 ± 0.02 (1.23)	0.02 ± 0.00 (2.64)	14.1 ± 1.8 (1.80)	14.4 ± 1.8 (2.01)	13.6 ± 1.6 (2.48)
Cerebellar cortex	0.29 ± 0.04 (0.85)	0.02 ± 0.00 (1.58)	13.9 ± 1.4 (1.05)	14.0 ± 1.4 (1.76)	13.2 ± 1.4 (0.61)
Total white matter	0.21 ± 0.02 (1.05)	0.04 ± 0.06 (2.28)	13.6 ± 1.8 (1.55)	14.0 ± 2.0 (1.55)*	13.5 ± 1.8 (1.20)

Presented as Mean \pm standard deviation, and mean percent standard error in parentheses

*One individual had poor fit for data from total white matter. The white matter data from this individual were excluded from the reported mean V_T for this region

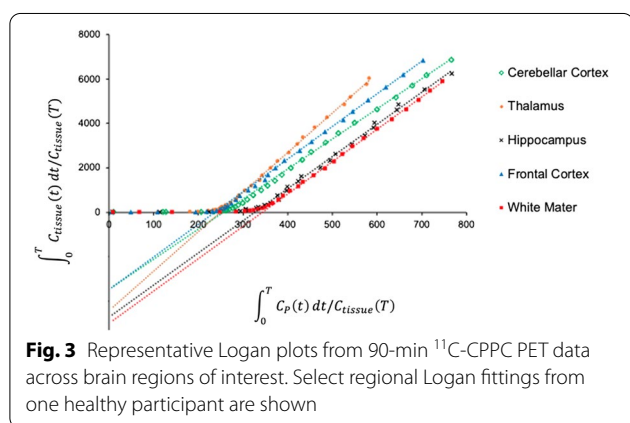


Fig. 3 Representative Logan plots from 90-min ^{11}C -CPPC PET data across brain regions of interest. Select regional Logan fittings from one healthy participant are shown

values (compartmental modeling, Logan) were relatively high in thalamus, striatum and most cortical regions, and lower in hippocampus, white matter, and cerebellar cortex. Parametric images of Logan-derived V_T are shown in Fig. 4 and Additional file 1: Fig. S2. With the exception of hippocampus, regional Logan-derived V_T values generated from truncated scan durations down to 65 min were within 5% of the V_T values obtained using 90-min emission data. In hippocampus, 75 min continuous scans were required to generate V_T within 5% of the V_T values obtained using the 90-min data (Fig. 5).

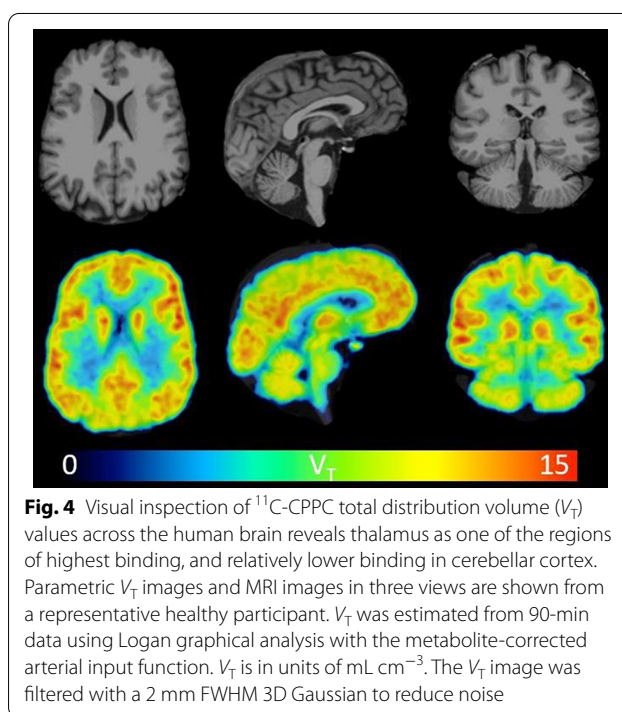
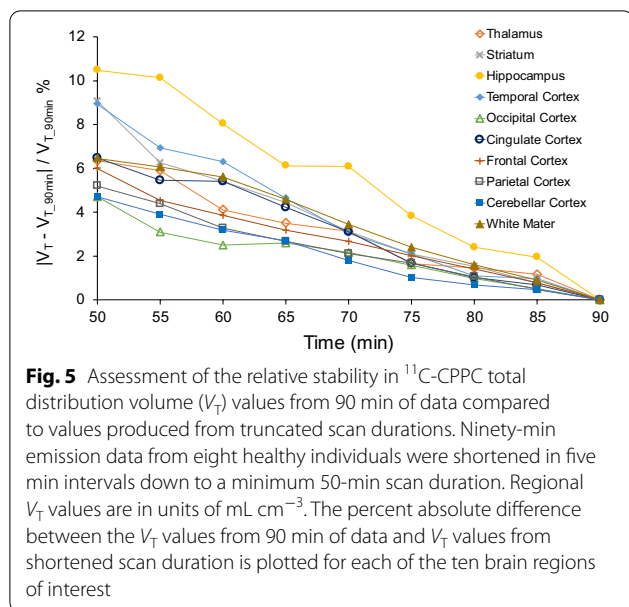


Fig. 4 Visual inspection of ^{11}C -CPPC total distribution volume (V_T) values across the human brain reveals thalamus as one of the regions of highest binding, and relatively lower binding in cerebellar cortex. Parametric V_T images and MRI images in three views are shown from a representative healthy participant. V_T was estimated from 90-min data using Logan graphical analysis with the metabolite-corrected arterial input function. V_T is in units of mL cm^{-3} . The V_T image was filtered with a 2 mm FWHM 3D Gaussian to reduce noise

Discussion

Study of the contribution of microglia to onset and course of several neuropsychiatric conditions is challenged by the fact that these brain-resident immune cells often appear and/or react differently in postmortem tissue compared to their native, in vivo micro-environment. Imaging microglia with radiotracers



developed for use with PET allows researchers to study these cells in the living human brain, and yet many relevant targets such as the 18 kDa translocator protein are also expressed on non-microglial cells. We developed ^{11}C -CPPC to image the CSF1R that is essentially expressed by microglia alone in the brain and present first-in-human evaluation of its pharmacokinetic behavior in the brains of healthy individuals.

The 2TCM estimated V_T well except for one unstable white matter V_T estimate from one individual. However, the 2TCM did not identify well several other parameters (k_2 , k_3 , k_4). The 2TCM was statistically favored over the 1TCM in 45% of fits by the F test, and yet regional V_T from 1TCM aligned with the well-identified V_T estimates from the 2TCM. Accordingly, the 1TCM was selected as the preferred compartmental model for ^{11}C -CPPC PET data. Further, Logan-derived regional V_T values aligned well with those from the 1TCM, supporting future use of Logan graphical analysis given the relative stability of Logan-derived V_T . Further, the majority of regional Logan-derived V_T values were well estimated using data from just 65 min acquisition, although the hippocampal region of interest was the exception and required 75 min of continuous data in order to generate V_T estimates that aligned well with the 90-min scan.

While several other CSF1R-targeting radiotracers have emerged for use with PET, to our knowledge ^{11}C -CPPC is the first used in humans. The future use of other CSF1R radioligands may be limited by evidence of poor brain penetrance in mice and nonhuman primates (^{11}C -AZ683) [22] or nonspecific binding (^{11}C -NCGG401)

[23]. Neuroimaging with ^{11}C -GW2580 PET has shown promising results in mouse models of neuroinflammation and in nonhuman primates, and yet brain uptake is lower than with ^{11}C -CPPC [24]. Future evaluation of ^{11}C -GW2580 pharmacokinetics in human brain is anticipated.

CSF1R is expressed by microglia across the brain, and there were no clear regions devoid of ^{11}C -CPPC uptake. In alignment with the reported expression pattern of CSF1R across the human brain [10], the highest V_T values were observed in thalamus, many cortical regions, and striatum, with moderate values in hippocampus and low V_T in cerebellar cortex. While CSF1R RNA has been reported as high in white matter [10], total white matter V_T values were low in these first eight healthy individuals. This observation may be due to the defined total white matter ROI in this study since reported RNA expression varies across white matter substructures [10]. The publicly available CSF1R RNA measures in human white matter were also obtained largely from individuals between the ages of 60–94 years, while the median age in the present study was 42 years. Future work should evaluate the CSF1R distribution across white matter regions in postmortem tissue from less elderly individuals and by assessing complementary ^{11}C -CPPC V_T estimates from white matter substructures.

Conclusion

This study supports further use of ^{11}C -CPPC with PET for measuring in vivo the CSF1R in the human brain. ^{11}C -CPPC showed high brain uptake across ROIs, and the 1TCM was selected as the preferred compartmental model for estimating regional V_T from 90-min emission data with a metabolite-corrected arterial input function. Logan-derived regional V_T estimates aligned well with those from the 1TCM. Given the ability to estimate regional V_T values well in health, it is also reasonable to pursue future evaluation of ^{11}C -CPPC with PET in clinical populations with microgliosis and/or microglial activation driving neurodegeneration.

Supplementary Information

The online version contains supplementary material available at <https://doi.org/10.1186/s13550-022-00929-4>.

Additional file 1: Fig. S1. Representative views of the ten regions of interest. **Fig. S2.** ^{11}C -CPPC total distribution volume (V_T) values across the human brain (N=8).

Acknowledgements

The authors would like to thank the technologists and managerial staff at the Johns Hopkins PET Center for assistance in the acquisition of these human PET data.

Author contributions

LS, AGH, JMC, YD, and MGP jointly developed the concept of the manuscript. LS, JMC, and YD together with RA, CKH, MKB, RO, AZ, and SES led the data acquisition. YD analyzed these imaging data. YW, DPH, AWH, WGL, RFD, and AGH jointly completed each radiotracer synthesis and the characterization of radiotracer dynamic behavior in blood plasma. All authors were involved in the writing and proof reading of the manuscript. All the authors read and approved the final manuscript.

Funding

This work was supported by the Hope for Depression Research Foundation, the Alzheimer's Drug Development Foundation, and the National Institutes of Health [MH125278 (JMC), EB024495 (MGP), AG066464 (AGH and MGP)].

Availability of data and materials

The datasets generated during and/or analyzed during the current study are available from the corresponding author on reasonable request.

Code availability

Not applicable.

Declarations**Ethics approval and consent to participate**

All procedures performed in studies involving human participants were in accordance with the ethical standards of the institutional and/or national research committee and with the 1964 Helsinki Declaration and its later amendments or comparable ethical standards. This article does not contain any studies involving animals. The study was approved by the Johns Hopkins Investigational Review Board and Radiation Safety Committees. All subjects provided written informed consent.

Consent for publication

Not applicable.

Competing interests

Under a license agreement between D&D Pharmatech and the Johns Hopkins University, the University, AGH, and MGP are entitled to royalty distributions related to the technology described in the study. MGP is a founder of and holds equity in D&D Pharmatech. He also is a paid consultant to the company. AGH is a paid consultant to the company. As the spouse of MGP, JMC shares his disclosures. This arrangement has been reviewed and approved by the Johns Hopkins University in accordance with its conflict of interest policies.

Author details

¹Department of Psychiatry and Behavioral Sciences, Johns Hopkins Medical Institutions, Baltimore, MD, USA. ²Russell H. Morgan Department of Radiology and Radiological Science, Johns Hopkins Medical Institutions, Baltimore, MD, USA.

Received: 8 June 2022 Accepted: 24 August 2022

Published online: 30 September 2022

References

- Kreisl WC, Kim MJ, Coughlin JM, Henter ID, Owen DR, Innis RB. PET imaging of neuroinflammation in neurological disorders. *Lancet Neurol*. 2020;19(11):940–50. [https://doi.org/10.1016/s1474-4422\(20\)30346-x](https://doi.org/10.1016/s1474-4422(20)30346-x).
- Notter T, Coughlin JM, Gschwind T, Weber-Stadlbauer U, Wang Y, Kassiou M, et al. Translational evaluation of translocator protein as a marker of neuroinflammation in schizophrenia. *Mol Psychiatry*. 2018;23(2):323–34. <https://doi.org/10.1038/mp.2016.248>.
- Janssen B, Mach RH. Development of brain PET imaging agents: strategies for imaging neuroinflammation in Alzheimer's disease. *Prog Mol Biol Transl Sci*. 2019;165:371–99. <https://doi.org/10.1016/bs.pmbts.2019.04.005>.
- Chen Z, Haider A, Chen J, Xiao Z, Gobbi L, Honer M, et al. The repertoire of small-molecule PET probes for neuroinflammation imaging: challenges and opportunities beyond TSPO. *J Med Chem*. 2021;64(24):17656–89. <https://doi.org/10.1021/acs.jmedchem.1c01571>.
- Narayanaswami V, Dahl K, Bernard-Gauthier V, Josephson L, Cumming P, Vasdev N. Emerging PET radiotracers and targets for imaging of neuroinflammation in neurodegenerative diseases: outlook beyond TSPO. *Mol Imaging*. 2018;17:1536012118792317. <https://doi.org/10.1177/1536012118792317>.
- Cătălin B, Stopper L, Bălșeanu TA, Scheller A. The in situ morphology of microglia is highly sensitive to the mode of tissue fixation. *J Chem Neuroanat*. 2017;86:59–66. <https://doi.org/10.1016/j.jchemneu.2017.08.007>.
- Notter T, Coughlin JM, Sawa A, Meyer U. Reconceptualization of translocator protein as a biomarker of neuroinflammation in psychiatry. *Mol Psychiatry*. 2018;23(1):36–47. <https://doi.org/10.1038/mp.2017.232>.
- Horti AG, Naik R, Foss CA, Minn I, Misheneva V, Du Y, et al. PET imaging of microglia by targeting macrophage colony-stimulating factor 1 receptor (CSF1R). *Proc Natl Acad Sci U S A*. 2019;116(5):1686–91. <https://doi.org/10.1073/pnas.1812155116>.
- Lin H, Lee E, Hestir K, Leo C, Huang M, Bosch E, et al. Discovery of a cytokine and its receptor by functional screening of the extracellular proteome. *Science*. 2008;320(5877):807–11. <https://doi.org/10.1126/science.1154370>.
- Uhlén M, Fagerberg L, Hallström BM, Lindskog C, Oksvold P, Mardinoglu A, et al. Proteomics. Tissue-based map of the human proteome. *Science*. 2015;347(6220):1260419. <https://doi.org/10.1126/science.1260419>.
- Akiyama H, Nishimura T, Kondo H, Ikeda K, Hayashi Y, McGeer PL. Expression of the receptor for macrophage colony stimulating factor by brain microglia and its upregulation in brains of patients with Alzheimer's disease and amyotrophic lateral sclerosis. *Brain Res*. 1994;639(1):171–4. [https://doi.org/10.1016/0006-8993\(94\)91779-5](https://doi.org/10.1016/0006-8993(94)91779-5).
- Lodder C, Scheyltjens I, Stancu IC, Botella Lucena P, Gutiérrez de Ravé M, Vanherle S, et al. CSF1R inhibition rescues tau pathology and neurodegeneration in an A/T/N model with combined AD pathologies, while preserving plaque associated microglia. *Acta Neuropathol Commun*. 2021;9(1):108. <https://doi.org/10.1186/s40478-021-01204-8>.
- Witcher KG, Bray CE, Chunchai T, Zhao F, O'Neil SM, Gordillo AJ, et al. Traumatic brain injury causes chronic cortical inflammation and neuronal dysfunction mediated by microglia. *J Neurosci*. 2021;41(7):1597–616. <https://doi.org/10.1523/jneurosci.2469-20.2020>.
- Bray CE, Witcher KG, Adekunle-Adegbite D, Ouvina M, Witzel M, Hans E, et al. Chronic cortical inflammation, cognitive impairment and immune reactivity associated with diffuse brain injury are ameliorated by forced turnover of microglia. *J Neurosci*. 2022. <https://doi.org/10.1523/jneurosci.1910-21.2022>.
- Illig CR, Chen J, Wall MJ, Wilson KJ, Ballentine SK, Rudolph MJ, et al. Discovery of novel FMS kinase inhibitors as anti-inflammatory agents. *Bioorg Med Chem Lett*. 2008;18(5):1642–8. <https://doi.org/10.1016/j.bmcl.2008.01.059>.
- Mathews WB, Wu Y, Horti AG, Naik R, Hall AW, Holt DP, et al. Radiosynthesis and validation of [5-cyano-N-(4-(4-[[[11C]methyl]piperazin-1-yl]-2-(piperidin-1-yl)phenyl]furan-2-carboxamide)] ([11C]CJCPCC), a PET radiotracer for imaging CSF1R, a microglia-specific marker. *J Labelled Compd Radiopharm*. 2019;62(13):903–8. <https://doi.org/10.1002/jlcr.3806>.
- Sossi V, Jong HWAMd, Barker WC, Bloomfield P, Burbar Z, Camborde ML et al. editors. The second generation HRRRT—a multi-centre scanner performance investigation. In: IEEE nuclear science symposium conference record, 2005; 2005.
- Rahmim A, Cheng JC, Blinder S, Camborde ML, Sossi V. Statistical dynamic image reconstruction in state-of-the-art high-resolution PET. *Phys Med Biol*. 2005;50(20):4887–912. <https://doi.org/10.1088/0031-9155/50/20/010>.
- Innis RB, Cunningham VJ, Delforge J, Fujita M, Gjedde A, Gunn RN, et al. Consensus nomenclature for in vivo imaging of reversibly binding radioligands. *J Cereb Blood Flow Metab*. 2007;27(9):1533–9. <https://doi.org/10.1038/sj.jcbfm.9600493>.
- Logan J, Fowler JS, Volkow ND, Wolf AP, Dewey SL, Schlyer DJ, et al. Graphical analysis of reversible radioligand binding from time-activity measurements applied to [N-11C-methyl]-(-)-cocaine PET studies in human subjects. *J Cereb Blood Flow Metab*. 1990;10(5):740–7. <https://doi.org/10.1038/jcbfm.1990.127>.
- Glatting G, Kletting P, Reske SN, Hohl K, Ring C. Choosing the optimal fit function: comparison of the Akaike information criterion and the F-test. *Med Phys*. 2007;34(11):4285–92. <https://doi.org/10.1118/1.2794176>.
- Tanzey SS, Shao X, Stauff J, Arteaga J, Sherman P, Scott PJH, et al. Synthesis and initial in vivo evaluation of [(11C)AZ683—a novel PET radiotracer for colony stimulating factor 1 receptor (CSF1R). *Pharmaceuticals (Basel)*. 2018. <https://doi.org/10.3390/ph11040136>.
- Ogata A, Ji B, Yamada T, Hattori S, Abe J, Ikenuma H, et al. [11C]NCGG401, a novel PET ligand for imaging of colony stimulating factor 1 receptors. *Bioorg*

Med Chem Lett. 2022;65:128704. <https://doi.org/10.1016/j.bmcl.2022.128704>.

24. Zhou X, Ji B, Seki C, Nagai Y, Minamimoto T, Fujinaga M, et al. PET imaging of colony-stimulating factor 1 receptor: a head-to-head comparison of a novel radioligand, (11)C-GW2580, and (11)C-CPPC, in mouse models of acute and chronic neuroinflammation and a rhesus monkey. *J Cereb Blood Flow Metab.* 2021;41(9):2410–22. <https://doi.org/10.1177/0271678x211004146>.

Publisher's Note

Springer Nature remains neutral with regard to jurisdictional claims in published maps and institutional affiliations.

Submit your manuscript to a SpringerOpen[®] journal and benefit from:

- ▶ Convenient online submission
- ▶ Rigorous peer review
- ▶ Open access: articles freely available online
- ▶ High visibility within the field
- ▶ Retaining the copyright to your article

Submit your next manuscript at ▶ [springeropen.com](https://www.springeropen.com)
